Journal of The Electrochemical Society

The Electrochemical Society
Advancing solid state & electrochemical science & technology

Internal Short Circuit Analysis of Cylindrical Lithium-Ion Cells Due to Structural Failure

Journal of The Electrochemical Society, 2021 **168** 030526

Internal Short Circuit Analysis of Cylindrical Lithium-Ion Cells Due to Structural Failure

Muhammad Sheikh,[1,z] Mohab Elmarakbi,[2] Sheikh Rehman,[3] and Ahmed Elmarakbi[2]

[1]*WMG, the University of Warwick, Coventry CV4 7AL, United Kingdom*
[2]*Department of Mechanical and Construction Engineering, Faculty of Engineering and Environment, Northumbria University, Newcastle NE18ST, United Kingdom*
[3] *the University of Sunderland, Faculty of Technology, Sunderland SR6 0DD, United Kingdom*

Battery failures are obvious after being subject to abuse conditions however predicting these failures in advance is crucial when using test and validation techniques to understand battery potential. Lithium-ion battery cells are widely used due to their high energy and power densities. When abusive conditions like the three-point bend loading are applied to lithium-ion batteries, what occurs to the mechanical behaviours and components is still mostly unknown. To further this understanding, this paper investigates the mechanical behaviour of the separator in the LiCoO2/Graphite cylindrical 18650 cells. Internal short circuit (ISC) behaviour, strain rate dependency, and electrochemical status of the cells (i.e. SOC dependency) are studied to understand failure patterns. Furthermore, a simple and effective constitutive model for the separator layer is formed, facilitating further mechanical analysis and numerical simulation of lithium-ion battery study. The occurrence of ISC is investigated by jellyroll deformation where the casing is removed, and quasi-static load is applied. A numerical simulation model is developed to further investigate sequential structural failures and temperature changes. Simulation results showed good accuracy with experimental results and are useful to predict structural failure of cells. The number of failures including electrolyte leakage, change in shape, sudden voltage drop/temperature rise, and gas venting is observed.
 [DOI: 10.1149/1945-7111/abec54]

Manuscript submitted December 2, 2020; revised manuscript received January 25, 2021. Published March 16, 2021.

The growth of the electric vehicle industry is required to help circumvent pollution and ensure emission control. This is why it is expected that 50% of the world's passenger vehicles will be electric by 2050.[1] With any new technology, it is important to identify potential challenges and be able to address them. The main areas of focus now are powertrain architecture, propulsion systems, control systems, and design. With regards to propulsion systems, the electric vehicle uses lithium-ion batteries which allows it to propel with great performance whilst having a long lifetime.[2] However, there are always risks associated with battery technology that can be mitigated to improve safety. Standard test procedures are also available to test batteries with minimizing risks where to characterise a lithium-ion battery, different testing techniques are used.[3–5] Some of the methods used, employ advanced equipment and tools including universal battery testers, advanced power supplies, accelerating rate calorimeter (ARC),[3,6] thermal chambers, IR thermography, and high-resolution cameras. Some of these techniques are combined with basic lab-based techniques, including characterisation at different charging and discharging rates, the variation of applied current and voltages, capacity estimation at different operating temperatures, and cell temperature estimation using thermocouples.[6–8] When it comes to short circuit study, it becomes a challenging task to consider these limitations. The purpose of an abuse test is to study and understand the lithium-ion battery's failure pattern and its mechanisms of failure. This paper studies the three-point bend mechanical loading condition and the associated failure patterns.

The short circuit phenomenon of the lithium-ion battery can be divided into various types but in general, is divided as an internal short circuit (ISC) or external short circuit (ESC). When cell terminals are shorted together outside the battery this refers to an external short circuit whilst an internal short circuit (ISC) develops inside the cell. ISC can be further divided into various types depending on the location and contact area. In Ref. 9 authors provided statistics of internal and external short circuits and documented that occurrence of ISC due to vehicle collision is 52% whereas the occurrence of ESC is 26%. The causes of ESC and ISC are different but over the period, they can result in similar failure patterns. ESC is often a result of a vehicle collision, battery pack or cell leakage, rollover, and abusive operating conditions. For instance, abnormal charge/discharge and operating temperatures. On the other hand, ISC development is more complicated. In Ref. 10 authors provided three types of ISC which are: mechanical abuse caused by damage/deformation of separator due to crushing, thermal abuse caused by the collapse of a separator due to excessive temperature, and electrical abuse where separator failure occurs as a result of dendrite growth due to overcharge or over-discharge.[11–14] The focus of this study is on mechanical and thermal abuse analysis of separator layers.

Various mechanical abuse conditions are considered for the ISC study and it was found that the type of loading has a great impact on failure pattern and severity.[15] The most common types of loading conditions used for short circuit studies are nail penetration, three-point bend, side-impact, and compression. All of the loading conditions can cause failure or damage to the separator, anode, and cathode, which can result in irreversible ISC.[16] Some Immediately notable failure patterns documented by Refs. 17–20 are sudden voltage drops, temperature rise, electrolyte leakage, venting gas, and chemical decomposition reactions, which can lead to thermal runaway or permanent damage to the battery.

In Refs. 21–23 various loading conditions are discussed, however, a full understanding of loading-dependent and electrochemical-dependent mechanical behaviours of lithium-ion battery components is essential for battery safety, optimization, and evaluation.[24]

A significant amount of work is done to understand cell failure at the micro and macro scales. We are only discussing micro-scale failures and the initiation of those failures within this work. Saharei et al.,[25–27] have conducted a series of experiments to understand the failure patterns of cylindrical cells and the evolution of stress using dog bone specimens. In Ref. 28, authors investigated the fracture analysis of particles on current collectors using the diffusion of lithium ions during charging and discharging.[29] In Ref. 30, the authors explained that the expansion of cathode/anode particles would cause grain fractures leading to battery capacity deterioration or sudden failure.[31] In Ref. 32, the authors reported that the charge/discharge would cause the exfoliation and failure of the SEI membrane[33] as well as the adhesive failure due to the electrode volume change.[34] In addition, the volume change of electrodes due

[z]E-mail: muhammad.sheikh@warwick.ac.uk

to intercalation/de-intercalation can introduce extra stress within the battery.[35] Although these all provide extensive failure information due to ISC, the fact remains that to recreate sequential failure is still a challenging task. Current studies primarily focus on the mechanical abusive conditions and analysis of ISC. For ISC initiation, nail penetration tests are widely conducted where voltage and temperature variations are studied to understand battery failures, but due to the unknown nature of the impact, it is necessary to study various shapes and sizes of the indenter. Three-point bend loading conditions create brutal failure scenarios, which range from fracture, buckling, rupture, or breaking of the cell. This study will investigate these avenues in detail as well as the mechanical aspects of separator failure due to three-point bend loading therefore the published work related to deep electrochemistry including electrolyte leakage or damage to the inner core is not discussed. ISC linking to mechanical and thermal abuse is further discussed where a numerical simulation approach is used to replicate these failures for the further study of the material properties. Finite element analysis (FEA) methods are commonly used by Refs. 25–28 and 36–41, which allows for the evaluation of the mechanical properties of battery specimens. This evaluation occurs where material properties are known, or sensitivity analysis can be used to determine these properties. In addition, lumped jellyroll models are considered to study failure patterns, but layer stacks are not considered, and individual material properties are not detailed. In Ref. 25 authors replicated fracture study using numerical simulation when temperature distribution across the layer is not considered. Within this paper, we have considered cell stacks with layer properties. Due to the limitation of electromagnetic (EM) solvers, electrochemistry is not included in the simulation work, and failures reported are a result of the mechanical and thermal solver. The role of testing batteries for the early detection of performance discrepancies for electric vehicle (EV) applications has encouraged the investigation of this significant issue in detail.

In this paper, failure analysis is conducted where two states of charge (SOCs) conditions (0% and 75%) are considered to analyse ISC of cylindrical 18650 cells. Separator failure criterion is used for further investigation of electrochemical failures where stress-strain and voltage-temperature relation is studied.

Experimental

Low capacity cells are chosen to avoid severe conditions during cell conditioning and actual tests. These cells have a steel casing of thickness ~0.30 mm and spiral wound layers of the: anode, cathode, separator, anode current collector, and cathode current collector.

A three-point bend test is performed on 18650 lithium-ion cells to check the mechanical integrity of these cells, to show where the cells bend when most of the stress is exerted on the mid-bottom surface. Three-point bend tests are not commonly used for these types of batteries, and very little evidence was found in Refs. 24–26 and Ref. 42, where the type of indenter and support varied in dimensions. The three-point bend test holder and indenter dimensions are given in Table I.

A Sharp edge with a thickness of 1 mm is selected for this study as it differs from the nail penetration tests. Whilst carrying out the study, sudden loading conditions were calculated which could be the result of the initial deformation of the separator layers. On the other hand, it could be the result of current collectors coming into contact and due to the energy absorption after short circuit forces drop down to low values and impact becomes quasi-static. The experimental setup is shown in Fig. 1.

Table I. Three-point bend indenter and holder dimensions.

Description	Dimensions
Cell holder length	88 mm
Cell holder width	56 mm
Cell holder cuts	19.7 mm
Bottom rigid plate thickness	4 mm
Gap between holder plates	42 mm
Indenter length	7.4 mm
Indenter thickness	1 mm
Indenter length	24.5 mm
Rod diameter	11.70 mm

The maximum force required to initiate a short circuit for 75% SOC is 2.98 kN, however lower force values are recorded at 0% SOC. Both a temperature increase and voltage drop were recorded for the two tests as shown in Fig. 2.

Temperature rise was sudden and rose at the rate of 700 °C min^{-1}. Sharp edge cracks occurred on the sides and mid surface as well as tension occurring at the bottom which showed the stiffness of the steel material at the time of impact. Similar results were observed for 0% SOC and 75% SOC. As shown in Fig. 3, initially the cell experienced an elastic region, but fractures occurred at a force of 2.5kN for 0% SOC and at 3.2kN the cell started to undergo deformation which is the initiation of ISC for this test. 75% more force was required for the initial fracture, which was 3.2kN, and permanent deformation occurred immediately after the initial fracture at 3kN and the cell experienced a short circuit. The buckling of the steel casing was observed when the force varied due to the softening of the steel casing but did not achieve permanent deformation.[42]

As explained above, a short circuit occurrence will be slow within high SOC cells, but temperature variation will be high due to the high-energy storage content. The rate of temperature change may vary depending on many factors including, the area of the fracture and the position of temperature measurement. In Fig. 3c, the voltage drop due to a short circuit is shown and it was observed that it took 7 s to attain the voltage drop to nearly zero value following the high temperatures attained. For the three-point bend test, nominal stress and nominal strain behaviour were calculated using Eqs. 1 to 4 as follows.[21]

$$\sigma_n = \frac{F}{A} \quad [1]$$

Where F is the force applied as shown and discussed in this chapter and previous chapters, A is the area of contact which is given by Ref. 42 as follows,

$$\mathrm{A} = l_c b_c \quad [2]$$

Where l_c is the length of the cell and width of the contact b_c, is calculated by Eq. 4.5, as given below,

$$\mathrm{b_c} = 2Rarc\cos\left[\frac{R - s/2}{R}\right] \quad [3]$$

Where "R" is the radius of the cell and "s" is the displacement of the indenter used, so the nominal stain ε_n can be obtained using Eq. 4.6, given as follow

$$\varepsilon_\mathrm{n} = \frac{s}{2R} \quad [4]$$

All the analyses mentioned in this section are discussed with each test protocol in the following section and the conclusion of the analysis is presented in the later section.

Immediate failure analysis.—Sharp edge indenter is used to investigate sharp object effect on cylindrical cells and possible thermal runaway events. At force (F_{t0}) which was 2.33kN a short circuit occurred during the 0% SOC test, where the complete discharge of the cell took 110 s. Short circuit displacement (d_{st0}) was 6.46 mm, and temperature change (ΔT_{t0}) was 16.3 °C. Table II gives the values of the parameters observed during the impact test.

Nominal stress-strain analysis.—As shown in Fig. 4a, nominal stress and nominal strain for battery degradation in the three-point bend test were observed where ε_{nt} represented nominal strain for three-point

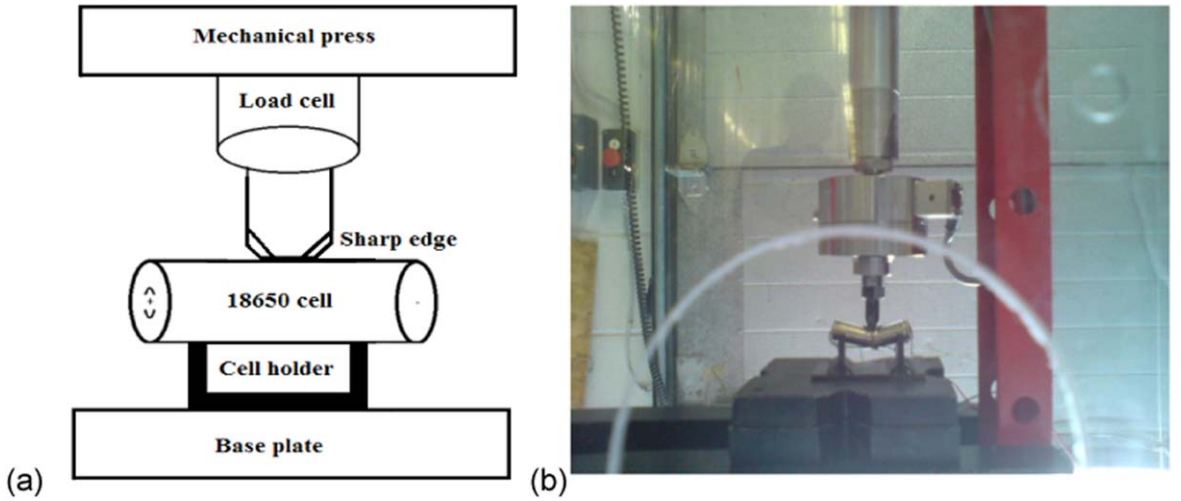

Figure 1. (a) Line diagram for Three-point test, (b) Experimental setup for Three-point bend test.

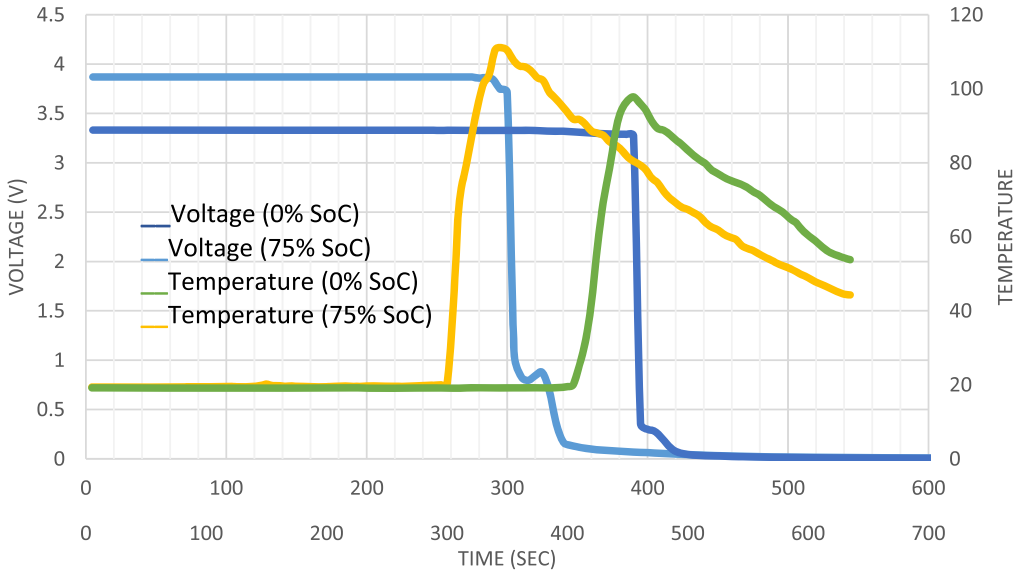

Figure 2. Voltage and temperature relation at the time of failure.

bend test, and σ_{nt} represented nominal stress for a three-point bend test. in regard to the case of the battery bending test, it indicates that the initial high-stress values were due to the steel casing buckling which in turn penetrates deep into the layers, and failure across the layers occurs. To better understand and generalise cell failure due to bending, failure strain for the three-point bend test is shown in Fig. 4b.

$$\varepsilon_{ft} = 0.34 - 0.0004\text{SOC} \quad [5]$$

Equation 5 shows a linear fit for the three-point bend test where ε_{ft} represents failure strain for the three-point bend test. Equation 5 has adjusted R square fit of 0.9384. As can be seen in Fig. 6, strain failure for the three-point bend test has linearly decreasing function where at lower SOC high strain failure was observed.

Figure 4c shows failure stress for the three-point bend test which is unlike the failure strain which was high at low SOCs. Linear fit for failure stress is given in Eq. 6, where σ_{ft} represents failure stress for the three-point bend test.

$$\sigma_{ft} = 2.0872 + 0.0095\text{SOC} \quad [6]$$

Post-failure structural analysis.—During the three-point bend test, cell bending and rupture were observed when the cell bent gradually. However, the formation of cracks was observed when the sharp edges were established in contact with the cell, shown in Fig. 5a. Both cell fracture and buckling take place in the three-point bend test when the sharp edge indenter is used. Cell terminals and end caps are intact in this testing; however, cell thinning took place at the centre of the cell. In this test, the indenter traveled 40% of the original cell diameter where the mean displacement is 7.27 mm.

Sideway deflection can be observed in the three-point bend, which is due to the triangular shape of the indenter tip. At cell failure, the fracture is observed in the three-point bend test where drastic temperature and voltage variations are observed.

Post-failure temperature analysis.—75% SOC is chosen for further analysis where the high-temperature change (ΔT_{t75}) and short circuit failure time (t_{t75}) are observed. In Fig. 5b, hotspot development is very slow and spans a period of time. The Hot spot is located at the bottom of the cell where temperature change was observed for 1 s and the heat dissipation effect is negligible.

(a)

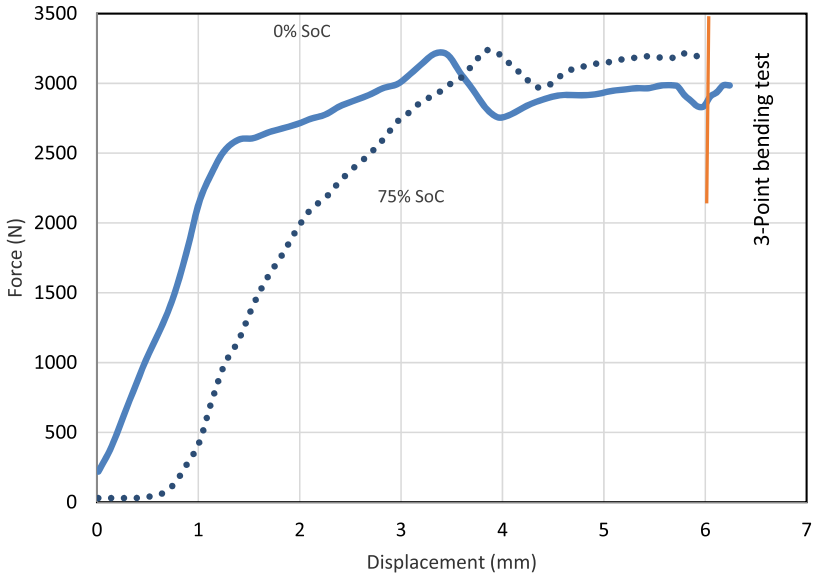

(b)

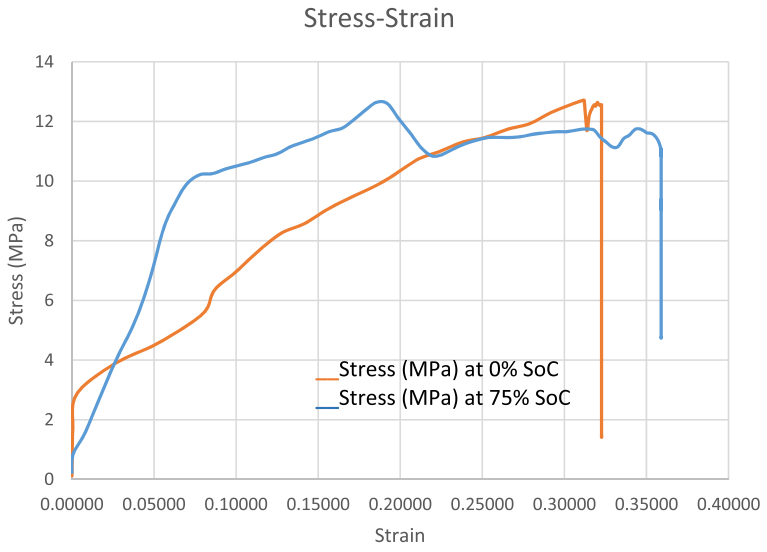

(c)

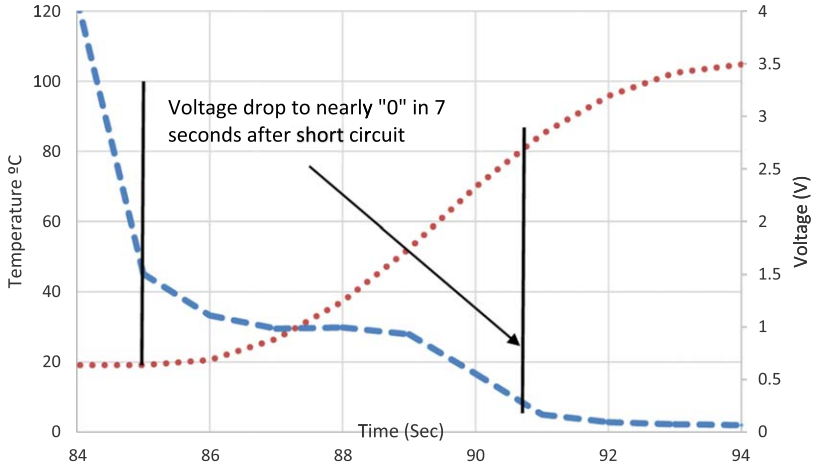

Figure 3. (a) Three-point bend test, Force and displacement relation at 0% and 75% SOCThree-point bend test, (b) Stress-Strain relation, (c) Sudden voltage drop as a result of short circuit due to bending.

In Fig. 5c, sample time with the temperature at the hotspot is shown, where the high-temperature location located at the bottom mid of the cell, unlike the commonly reported bending and fracture pattern for the three-point bend test. Due to the indenter shape, the cell showed fractures on the top surface and bending at the bottom.

Table II. Rod test results at short circuit development.

SoC	Time (Sec) t_r	Force (KN) F_r	Displacement (mm) d_{sr}	Initial temp (°C) T_{ir}	Final temp (°C) T_{fr}	Change in temp (°C) ΔT_r	Voltage Vi_r	Nominal failure Strain ε_{nr}	Nominal failure stress, σ_{nr} (MPa)
0%	280	10.32	8.389	20.0	25.30	5.30	3.343	0.4661	8.754
75%	310	12.25	6.971	21.3	107.5	86.20	3.894	0.3870	11.490

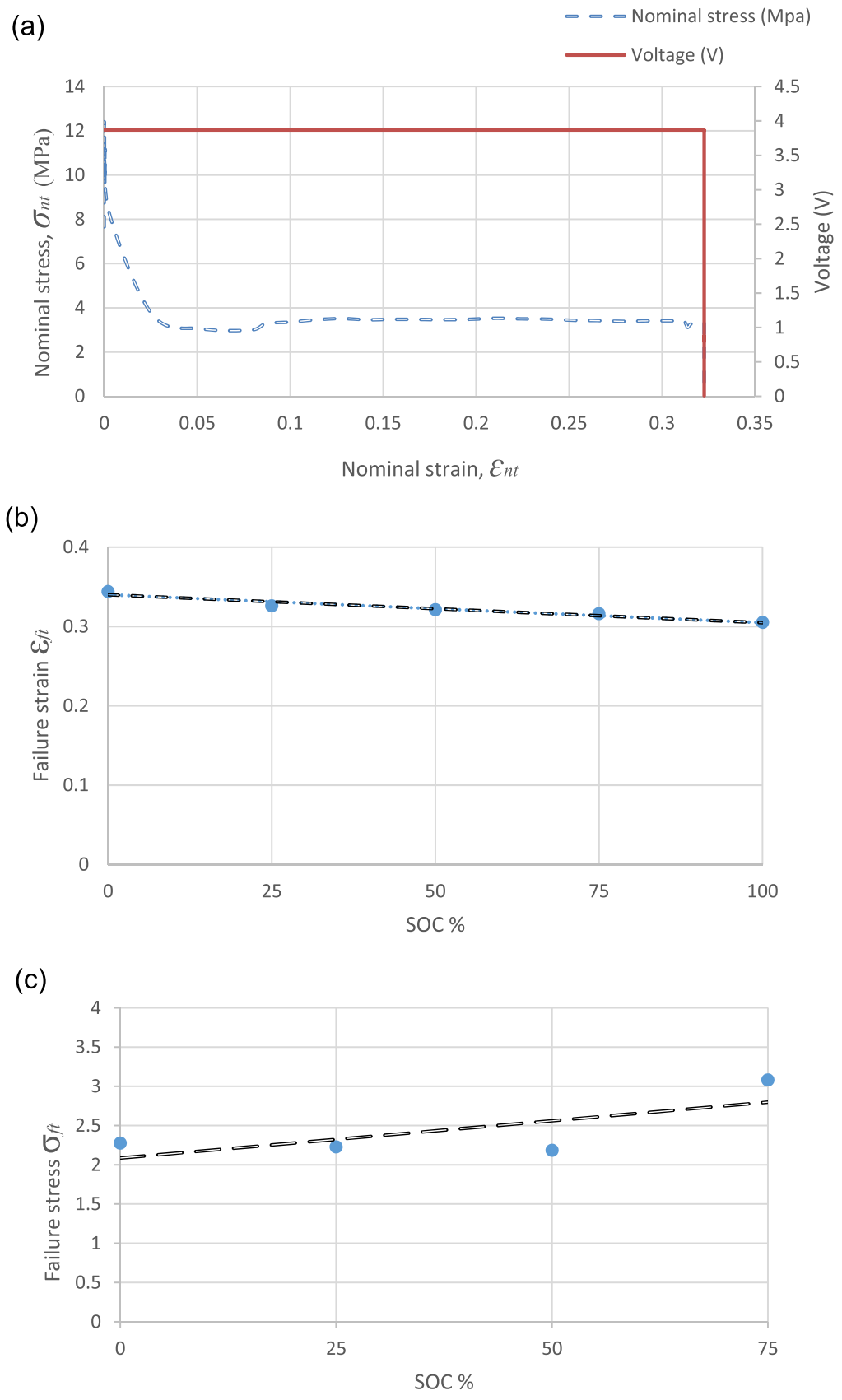

Figure 4. (a) Three-point bend test, Nominal stress-strain and voltage-strain curve, (b) Nominal failure strain for three-point bend test, (c) Nominal failure stress for a three-point bend test.

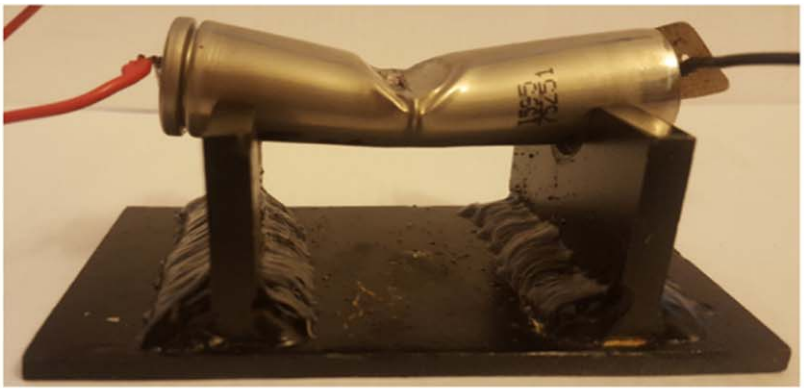

(a)

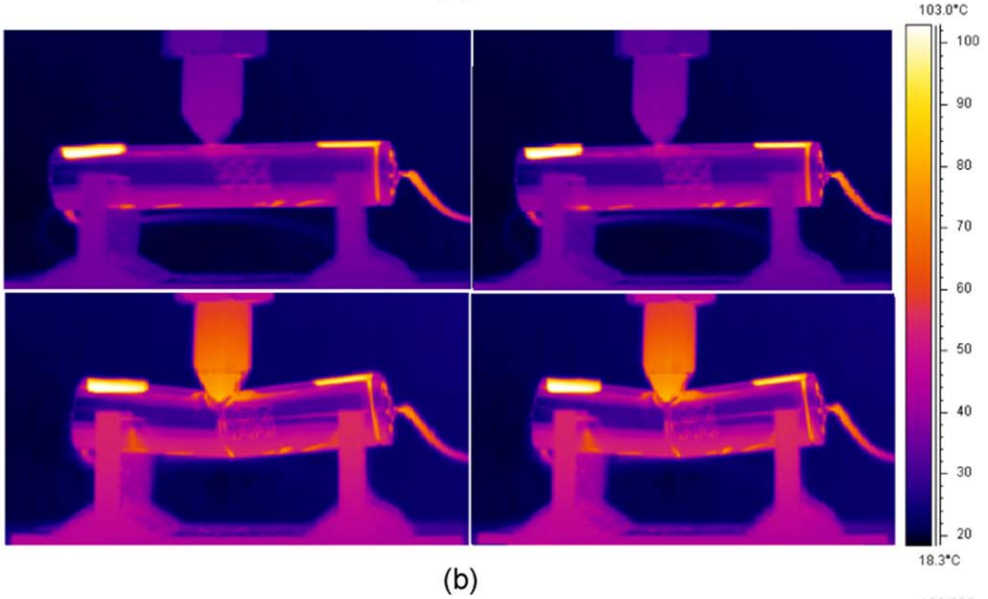

(b)

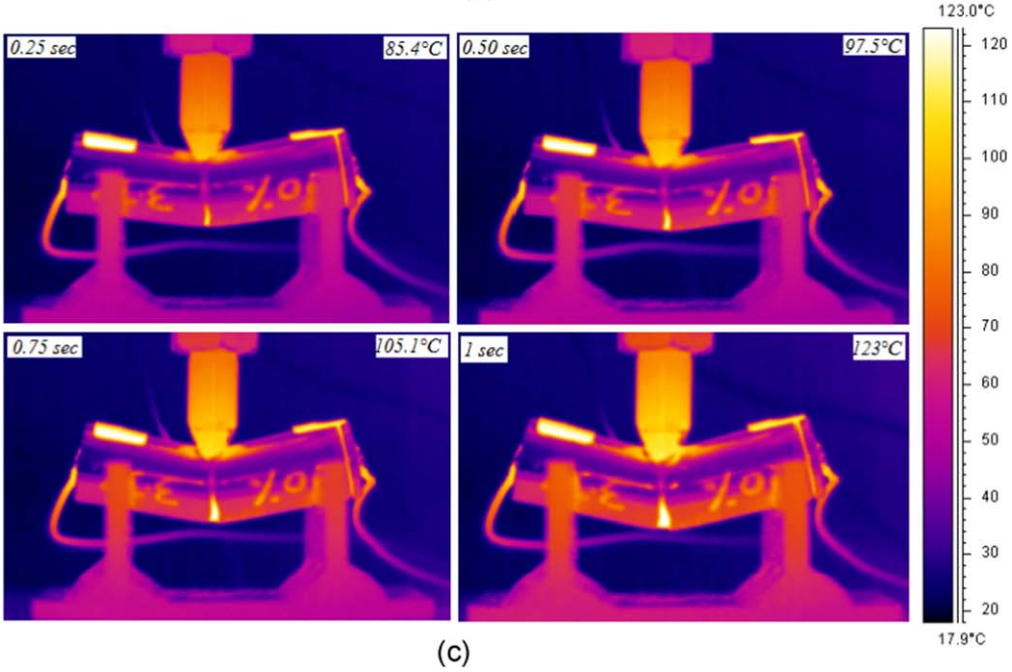

(c)

Figure 5. (a) Three-point bend test, (b) Initial results of temperature change for three-point bend test, (c) Initial temperature change with sample time for a three-point bend test.

Table III. Material properties used for LS-DYNA simulation.[46–51]

Material	Mass density (Tonne/mm^3)	Modulus of elasticity (MPa)	Poisson ratio	Yield stress (MPa)	% Failure strain ε_f
Copper current collector	7.94e-9	1.1e5	0.35	210	5
Aluminum current collector	2.69e-9	7e4	0.36	180	5
Anode	2.23e-9	1e4	0.3	100	10
Cathode	4.20e-9	1e4	0.3	100	10
Separator	1.179e-9	3.45e3	0.35	18	25
Steel casing	7.83e-9	2e5	0.3	450	4
Rigid plate	—	—	—	—	

Cylindrical 18650 lithium-ion battery's homogeneous jellyroll models are found in the current literature, which addresses the battery failures for quasi-static and dynamic simulations. However detailed layered models, which are equally important to understand sequential failures due to mechanical loading conditions, are not found in detail. Within this paper battery, layered models are developed using the LS-DYNA simulation tool and the results are validated.

Validation of Experimental Results

A layered battery model is chosen. The purpose of choosing an alternative model is to verify results on a small scale compared to the lithium-ion cell model where the number of elements is much higher which increases computation time. Making it sometimes difficult to rectify issues if a complete cell model is encountered comprised of several settings and conditions. For the initial model mainly three material types are used, where for the separator, anode, and cathode MAT_63_CRUSHABLE_FOAM is used. The crushable foam material is used as it has an option of tension cut off where tension is treated as elastic-perfectly-plastic at the tension cut-off value.[43] Detailed validation of crushable foam is given by Ref. 44. For the current collectors and steel casing MAT_24_PIECEWISE_LINEAR_PLASTICITY is used. Piecewise linear plasticity material model accounts for stress-strain behaviour where a curve can be used to provide stress-strain values. For the rigid base plate, MAT_20_RIGID is used to turn the solid element part into a rigid body. Detailed properties and relevant characteristics of materials used can be found in the LS-DYNA material model manual.[45] Element size selection is crucial which affects computation efficiency as well as stability of the model. Material properties for current collectors and active materials are used from Refs. 45–49 and experimental study, which is given in Table III.

Formation of the concentric layered model.—In Ref. 52 authors mentioned 304 layers for 18650 cells which account for 38 stacks, where each stack contains eight layers. To model 304 layers with exact thickness requires high computation efficiency and modelling time, where very thin layers need special modelling precautions. Within this research, the concentric layer-model formation was used to model 18650 cylindrical cell, which was not found in the literature, however, the jellyroll model where all the layers are lumped in the jellyroll model was proposed by Ref. 26. As cells have a spiral wound formation in general, a concentric layer model represents a different structure, where the main aim is to find an alternative way to model the battery where each layer is independent in regards to geometry. However, layers share mechanical and thermal behaviour under loading conditions. A thicker layer model is found to be the best choice to represent cells with the number of layers.[48–50]

In this paper all layers are considered to be the same size, this assumption provides an opportunity for simplifying the model as well as, due to the low thickness compared to Refs. 48, 49, more layers can be integrated to form a complete cell. The Steel casing has an almost similar size to the original cell. Concentric layers can be an appropriate alternative to spiral-wound layers, which are complex to design and simulate due to the different thicknesses of the cell layers.

Simulation parameters and assumptions.—The initial cell temperature selected was 22 °C, which is in agreement with single-cell testing standards and SAEJ2464 standard, which sets the limit of 55 °C for module-level tests. The battery model is modelled with a fully integrated solid element formulation, where a total of 103306 elements are used. The size of elements for steel casing is 0.5 mm and for all other layers is 1 mm. The reason for different element size selection is to achieve accuracy, where steel housing is the first layer to experience load. All indenters and bottom plates are modelled as rigid geometry, where the rigid material MAT_20_RIGID was used. A coefficient of friction between cell

Table IV. LS-DYNA consistent units.

Consistent units (Steel material)

Mass	Length	Time	Force	Stress	Energy	Density	Young's Modulus
ton	*mm*	*s*	*N*	*MPa*	*N-mm*	(Tonne mm^{-3})	*MPa*

Table V. Cell heat capacity and thermal conductivity parameters for the simulation.

Type of layer	Heat capacity (Jkg^{-1}K^{-1})	Thermal conductivity (Wm^{-1}K^{-1})
Steel shell casing	477	14.9
Separator	1978	0.334
Anode active material	700	5
Cathode active material	700	5
Anode current collector	386	400
Cathode current collector	900	200

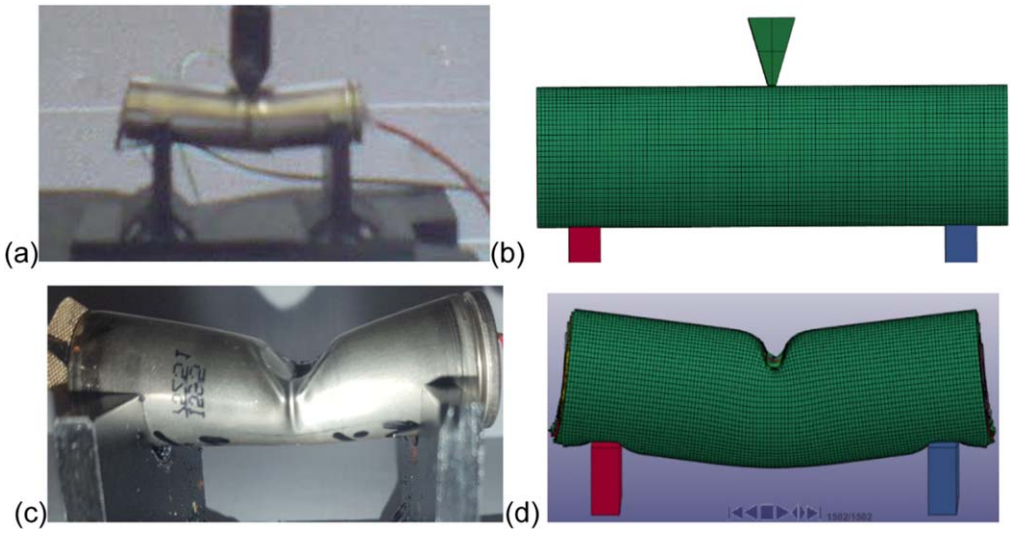

Figure 6. Three-point bend test, (a) undeformed test, (b) undeformed simulation, (c) deformed test results quasi-static load, (d) deformed simulation results quasi-static load.

and support is considered to be 0.3 as given by in Ref. 25. No endcaps were taken into account for this simulation, however, SPC boundary conditions were used to restrain components of the battery if required. Failure strain of the separator documented by Ref. 49 was 93%; however, separator failure strain of 35% to 80% from the literature is evident, which means values of 0.2 to 0.5 (50% or 80%

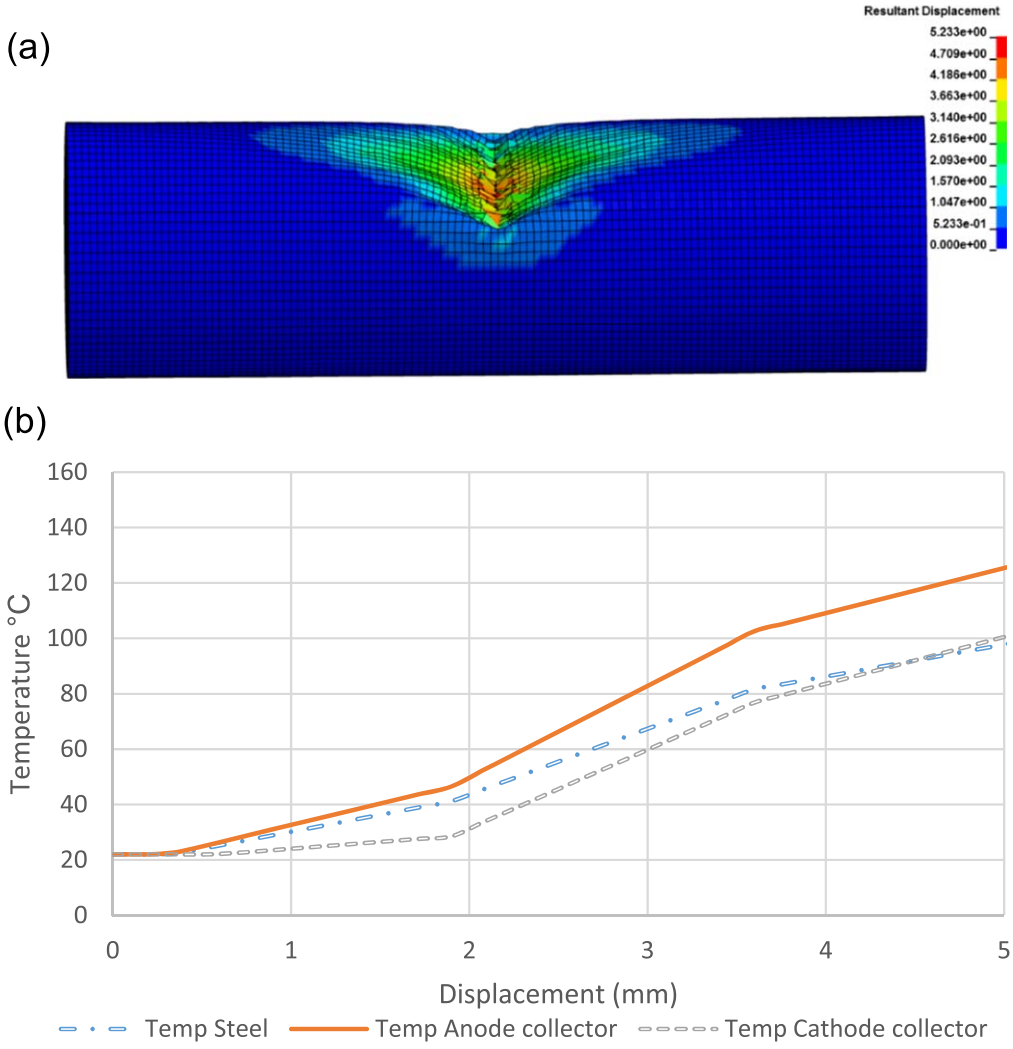

Figure 7. (a) Resultant displacement due to quasi-static load, (b) Temperature values for steel casing, anode current collector, and cathode current collector.

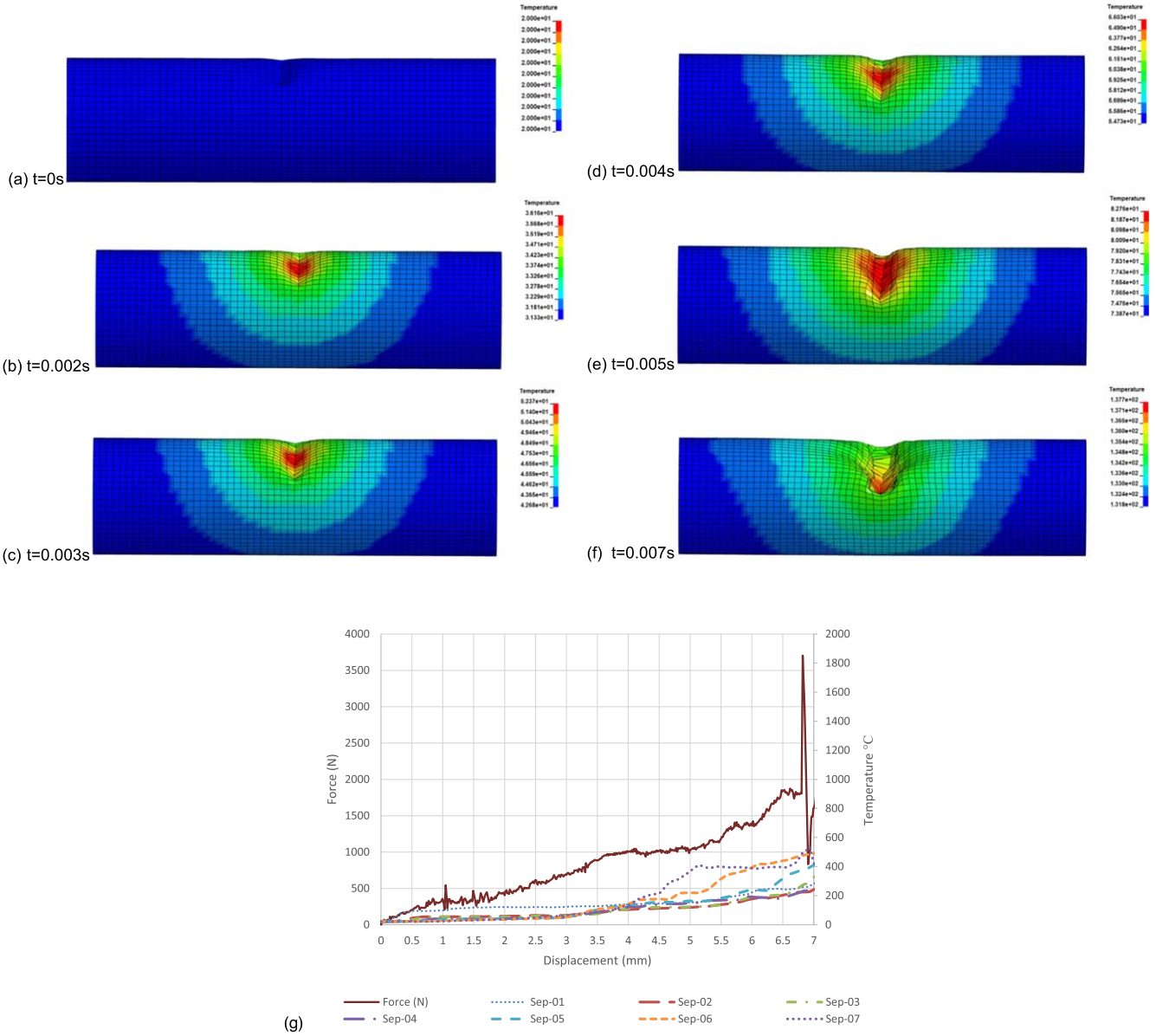

Figure 8. (a) to (f) Three-point bend simulation, temperature variations at the first separator layer, (g) Separator layers behavior with applied force, displacement, and temperature variations.

of initial thickness) could be used for the separator. Consistent units by (LSD-DYNA consistent units) were used for all simulation models given in Table IV.

Cylindrical 18650 cell simulation model.—Based on the above-mentioned properties and assumptions, the simulation model is designed to understand the loading impact on the cell for separator failure analysis. For simulation, all layers (steel shell casing, anode, cathode, separators, anode current collector, and cathode current collector) were considered to be 0.3 mm thick, and the innermost radius was considered to be 1 mm as detailed in Ref. 53. It is important to understand the material properties for the individual layers for stress/strain relation and for that purpose, two foam material models were discussed in Ref. 26 and the three-point bend test was considered for the initial investigation. True stress/strain curve from the dogbone specimen for the shell casing is given and nominal failure stress and failure strain were used from the experimental results, where for each test case values at 0% SOC was used, which is to check if the model predicts failure. The steel casing material is modelled using MAT-24-PIECEWISE-LINEAR-PLASTICITY in LS-DYNA. The Separator, anode, and cathode were considered to be the MAT-63-CRUSHABLE-FOAM model, and the anode current collector and cathode current collector were modelled using MAT-003-PLASTIC-KINEMATIC. The stress/strain curve for the separator, active anode material, and active cathode material was used from Refs. 49 and 53. Coupled mechanical and thermal solver is used, where structural deformation is an input for the thermal solver. Heat capacity and thermal conductivity of individual layers are given in Table V.

Boundary prescribed motion set is used in this simulation to define object motion throughout the simulation at every single time step. Due to the sensitive nature of contact cards, accurate contact interface modelling is necessary which improves finite element simulation results.

Three-point bend test simulation.—For the three-point bend test simulation, cell holders and the sharp edge are modelled using rigid materials. The numerical simulation model for the three-point bend and experimental and simulation geometries for pre and post-loading are shown in Fig. 6.

Initially, when the load was applied on the cylindrical cell it used less force for compression but after some time due to the material

hardening, excessive force was required for compression. Short circuit displacement was observed at 5.23 mm for quasi-static analysis Fig. 7a shows resultant displacement due to quasi-static loading.

As can be seen from Fig. 7a, sideways buckling of steel casing is found due to the sharp edge cell fracture is at the point of contact of the sharp edge. For the three-point bend test simulation comparison of steel, anode current collector and cathode current collector layers are used to understand the temperature distribution of the cell for the internal layers, where the anode current collector and cathode current collector indicates the first instance of short circuit. The negative electrode has a high thermal conductivity so the temperature change at the anode current collector is high compared to the cathode current collector.

As can be seen from Fig. 7b, the temperature for the steel and cathode current collector (aluminum) is around 100 °C; however, the temperature for the anode current collector is around 130 °C at the time of short circuit occurrence.

Separator failure analysis.—The three-point bend test short circuit failure was further analysed using separator failure criteria, where all separator layers were examined for their temperature variations. Separator layer temperature variations are shown in Fig. 8.

The top surface of the separator layer 1, is shown for deformation and temperature variation with regards to location. For separator layer 1, sideways deflection and temperature variation are shown. Due to sharp-edge, cell damage occurs relatively early compared to other loading cases, which sequentially damages layers within the cell. Due to both the tension and compression separator layers having low mechanical strength brittle fractures develops, which occurs immediately after the steel casing fracture and temperature increases drastically as shown within the experiment work and this simulation model. Layer behaviour due to the applied force is provided in Fig. 8b.

The simulation model results show good accuracy within the cell comparison. During lithium-ion battery construction the separators have the lowest melting point and melt at around 144 °C,[49] so separator failure may occur earlier compared to other layer failures which have comparatively high melting points. This separator failure is also an indication of ISC as contact between electrodes is established once separator layers melt. As shown in Fig. 8a to 8f, force attains the same peak value as documented in the experimental section for the three-point bend, however, a sudden drop in force at around 7 mm pinpoints the short circuit occurrence. The Temperatures of all layers started to increase after the short circuit and the last separator layer which is sep-07 experiences a temperature drop, which is stabilising zone or short circuit propagation. Once the thermal runaway occurred temperature started to increase in an uncontrolled manner, and the temperature of all the layers was around 300 °C except sep-05 to sep-07 which attain temperatures of around 500 °C for a short instance of time. Sep-07 layer experienced high compression and tension due to the three-point bend as forces from all other layers and indenter were applied at this layer, where the layer shrinks and element deletion takes place. Separator analysis with high-temperature variations can be used as an indicator of ISC or initial cell failure.

Conclusions

Internal short circuit (ISC) behaviour, strain rate dependency, and electrochemical status of the cells (i.e. SOC dependency) are studied to understand failure patterns. The occurrence of ISC is investigated by jellyroll deformation where the casing is removed, and quasi-static load is applied. The numerical simulation model is used to investigate sequential structural failures and temperature changes. Simulation results showed good accuracy with experimental results and are useful to predict structural failure of cells. Immediate failures like electrolyte leakage, change in shape, sudden voltage drop/temperature rise, and gas venting are observed. The location and intensity of the short circuit, time for the initial and complete failure of cells, and structural deformation were considered in detail as well as using simulation models to analyse separator failures. One of the significant findings from this research is that at maximum displacement separator temperature increased significantly and a drop in force was observed. The time of short circuit and force drop was due to the internal stiffness of layers where temperature started to increase, but high temperatures, which were uncontrolled lead to severe failures. Another significant finding from separator layer analysis is that there were high-temperature locations, which indicate electrochemical changes due to internal short circuits. Furthermore, separator failure occurs well in advance for the short circuit for the three-point bend test, which has an immediate short circuit response. The failure response of the separators is in agreement with the experimental work where the failure of the layers took place for the three-point bend, and all separator layers showed high temperatures and changes in their shape.

ORCID

Muhammad Sheikh https://orcid.org/0000-0003-4019-7031

References

1. A. Abaza, S. Ferrari, H. K. Wong, C. Lyness, A. D. Moore, J. Weaving, M. Blanco-Martin, R. Dashwood, and R. Bhagat, "Experimental study of internal and external short circuits of commercial automotive pouch lithium-ion cells." *Journal of Energy Storage*, **16**, 211 (2018).
2. M. Dubarry and G. Baure, "Perspective on commercial Li-ion battery testing, best practices for simple and effective protocols." *Electronics (Switzerland)*, **9**, 1 (2020).
3. M. Sheikh, A. Elmarakbi, and S. Rehman, "A combined experimental and simulation approach for short circuit prediction of 18650 lithium-ion battery under mechanical abuse conditions." *Journal of Energy Storage*, **32**, 101833 (2020).
4. J. E. Harlow et al., "A wide range of testing results on an excellent lithium-ion cell chemistry to be used as benchmarks for new battery technologies." *J. Electrochem. Soc.*, **166**, 3031 (2019).
5. W. Porcher, M. Montaru Cidetec Mikel Arrinda Martinez, A. Marongiu, M. F. Oyarbide Jülich Niloofar Ehteshami TU München Yao Wu HI Ulm Arianna Moretti, S. Passerini, and G. Jan Berckmans ViF Philip Kargl, "Draft White paper Test methods for improved battery cell understanding." (2017).
6. V. Ruiz, A. Pfrang, A. Kriston, N. Omar, P. Van den Bossche, and L. Boon-Brett, "A review of international abuse testing standards and regulations for lithium ion batteries in electric and hybrid electric vehicles." *In Renewable and Sustainable Energy Reviews*, **81**, 1427 (2018).
7. A. Tomaszewska et al., "Lithium-ion battery fast charging: a review." *ETransportation.*, **1**, 28 (2019).
8. G. Zhang, L. Cao, S. Ge, C. Y. Wang, C. E. Shaffer, and C. D. Rahn, "In situ measurement of radial temperature distributions in cylindrical li-ion cells." *J. Electrochem. Soc.*, **161**, A1499 (2014).
9. D. Doughty and E. P. Roth, "A general discussion of li-ion battery safety." *The Electrochemical Society Interface, summer*, **2012**, 37 (2012).
10. L. Lu, X. Han, j. Li, J. Hua, and M. Ouyang, "A review on the key issues for lithium-ion battery management in electric vehicles." *J. Power Sources*, **226**, 272 (2013).
11. H. Budde-Meiwes, J. Drillkens, B. Lunz, J. Muennix, S. Rothgang, J. Kowal, and D. U. Sauer, "A review of current automotive battery technology and future prospects." *Proc. Inst. Mech. Eng. Part D J. Automob. Eng.*, **227**, 761 (2013).
12. R. Kizilel, R. Sabbah, J. R. Selman, and S. Al-Hallaj, "An alternative cooling system to enhance the safety of li-ion battery packs." *J. Power Sources*, **194**, 1105 (2009).
13. K. A. Smith, C. D. Rahn, and C. Y. Wang, "Control oriented 1D electrochemical model of lithium ion battery." *Energy Convers. Manage.*, **48**, 2565 (2007).
14. C. Julien, A. Mauger, K. Zaghib, and H. Groult, "Optimization of layered cathode materials for lithium-ion batteries." *Materials*, **9**, 595 (2016).
15. H. He, R. Xiong, H. Guo, and S. Li, "Comparison study on the battery models used for energy management of batteries in electric vehicles." *Energy Convers. Manage.*, **64**, 113 (2012).
16. R. Zhao, J. Gu, and J. Liu, "An investigation on the significance of reversible heat to the thermal behavior of lithium ion battery through simulations." *J. Power Sources*, **266**, 422 (2014).
17. G. Albright and S. Al-Hallaj, "Making lithium-ion safe through thermal management." (2012), (http://battcon.com/PapersFinal2012/Greg%20Albright%20-).
18. D. Lisbona and T. Snee, "A review of hazards associated with primary lithium and lithium-ion batteries." *Journal of Process Safety and Environmental Protection*, **89**, 434 (2011).
19. Y. Shi, D. J. Noelle, M. Wang, A. V. Le, H. Yoon, M. Zhang, Y. Meng, and Y. Qiao, "1Exothermic behaviors of mechanically abused lithium-ion batteries with dibenzylamine." *J. Power Sources*, **326**, 514 (2016).
20. J. M. Miller, "Energy storage system technology challenges facing strong hybrid, plugin and battery electric vehicles." *Proceedings of IEEE, Vehicle Power and Propulsion Conference, VPPC '09. 7–10 Sept. 2009*, Dearborn, MI, United States of America (2009).

21. M. Sheikh, A. Elmarakbi, and M. Elkady, "Thermal runaway detection of cylindrical 18650 lithium-ion battery under quasi-static loading conditions." *J. Power Sources*, **370**, 61 (2017).
22. M. Sheikh, A. Elmarakbi, and S. Rehman, "A combined experimental and numerical simulation approach to predict short circuit due to mechanical abuse conditions." *Journal of Energy Storage*, **32**, 101833 (2020).
23. M. Sheikh, S. Rehman, and M. Elkady, "Numerical simulation model for short circuit prediction under compression and bending of 18650 cylindrical lithium-ion battery." *Journal of Energy Procedia*, **151**, 187 (2018).
24. G.-H. Kim, A. Pesaran, and R. Spotniz, "A three dimensional thermal abuse model for lithium-ion cells." *J. Power Sources*, **170**, 476 (2007).
25. E. Sahraei, R. Hill, and T. Wierzbicki, "Calibration and finite element simulation of pouch lithium-ion batteries for mechanical integrity." *J. Power Sources*, **201**, 307 (2012a).
26. E. Sahraei, M. Kahn, J. Meierc, and T. Wierzbicki, "Modelling of cracks developed in lithium-ion cells under mechanical loading." *Royal Society of Chemistry Advances*, **5**, 80369 (2015).
27. E. Sahraei, T. Wierzbicki, R. Hill, and M. Luo, "Crash safety of lithium-ion batteries towards development of a computational model'." SAE Technical paper 2010-01-1078, Detroit, Michigan USA, April 13–April 15, 2010 (2010).
28. E. Sahraei, J. Campbell, and T. Wierzbicki, "Modeling and short circuit detection of 18650 Li-ion cells under mechanical abuse conditions." *J. Power Sources*, **220**, 360 (2012b).
29. C. Lopez, J. Jeevarajan, and P. Mukherjee, "Characterization of lithium-ion battery thermal abuse behavior using experimental and computational analysis." *Journal of Electrochemical Society*, **162**, A2163 (2015).
30. S. J. Bazinski and X. Wang, "Experimental study on the influence of temperature and state-of-charge on the thermophysical properties of an LFP pouch cell." *J. Power Sources*, **293**, 283 (2015).
31. N. S. Spinner, R. Mazurick, A. Brandon, S. L. Rose-Pehrsson, and S. G. Tuttle, "Analytical, numerical and experimental determination of thermophysical properties of commercial 18650 licoo2 lithium-ion battery." *J. Electrochem. Soc.*, **162**, A2789 (2015b).
32. L. Siguang and Z. Chengning, "Study on battery management system and lithium-ion battery." *Proceedings of IEEE, International Conference on Computer and Automation Engineering (ICCAE '09),* 8–10 March 2009, Bangkok, Thailand (2009).
33. R. R. Richardson, P. T. Ireland, and D. A. Howey, "Battery internal temperature estimation by combined impedance and surface temperature measurement." *J. Power Sources*, **265**, 254 (2014).
34. Y. Chen and J. W. Evans, "Thermal analysis of Lithium-Ion batteries." *Journal of Electrochemical Society*, **143**, 2708 (1996).
35. G. H. Kim and A. Pesaran, *Fifth International Symposium on Large Lithium Ion Battery Technology and Application. June 9-10, 2009* (Long Beach Convention Center, Long Beach, CaliforniaL, CA) (2009).
36. J. Marcicki, M. Zhu, A. Bartlett, X. G. Yang, Y. Chen, T. Miller, P. L'Eplattenier, and I. Caldichoury, "A simulation framework for battery cell impact safety modeling using LS-DYNA." *J. Electrochem. Soc.*, **164**, A6440 (2017).
37. W. W. Wang, S. YANG, and C. Lin, "Clay-like mechanical properties of components for the jellyroll of cylindrical lithium-ion cells." *Energy Procedia*, **104**, 56 (2016).
38. Y. Xia, T. Wierzbicki, E. Saharei, and X. Zhang, "Damage of cells and battery pack due to ground impact." *J. Power Sources*, **267**, 78 (2014).
39. G. Trattnig and W. Leitgeb, "Automotive Engineering. Simulation and Validation Methods." *Battery Modelling for Crash Safety Simulation* (Virtual Vehicle Research Center, Graz, Austria) (2014).
40. T. Wierzbicki and E. Sahraei, "Homogenized mechanical properties for the jellyroll of cylindrical Lithium-ion cells." *J. Power Sources*, **241**, 467 (2016).
41. E. Martínez-Rosas, R. Vasquez-Medrano, and A. Flores-Tlacuahuac, "Modeling and simulation of lithium-ion batteries." *Comput. Chem. Eng.*, **35**, 1937 (2011).
42. J. Xu, B. Liu, and D. Hu, "State of charge dependent mechanical integrity behavior of 18650 lithium-ion batteries." *Sci. Rep.*, **6**, 21829 (2016).
43. Material selector for LS-DYNA, "2. LSTC website." (Accessed on June 2016) (2016) (http://lstc.com/dynamat/).
44. G. Slik, G. Vogel, and V. Chawda, *Material Model Validation of a High Efficient Energy Absorbing Foam* (5th LS-DYNA forum) 12–13 October 2006, (Ulm, Germany) (2006).
45. M. Sheikh, S. Rehman, and M. Elkady, "Numerical simulation model for short circuit prediction under compression and bending of 18650 cylindrical lithium-ion battery." *Energy Procedia*, **151**, 187 (2018).
46. LS-DYNA keyword user's manual, volume (ii) material models, LSTC, LS-DYNA R8.0, (Accessed June) (2016) (http://www.dynasupport.com/manuals/ls-dyna-manuals/ls-dyna-manual-r-8.0-vol-ii).
47. The Engineering tool box, (Accessed on May 2017) (2017) (http://www.engineeringtoolbox.com/young-modulus-d_417.html).
48. C. Zhang, S. Santhanagopalan, M. A. Sprague, and A. A. Pesaran, "Coupled mechanical-electrical-thermal modeling for short-circuit prediction in a lithium-ion cell under mechanical abuse." *J. Power Sources*, **290**, 102 (2015).
49. C. Zhang, S. Santhanagopalan, M. A. Sprague, and A. A. Pesaran, "A representative-sandwich model for simultaneously coupled mechanical-electrical-thermal simulation of a lithium-ion cell under quasi-static indentation tests." *J. Power Sources*, **298**, 309 (2015).
50. E. Sahraei, J. Meier, and T. Wierzbicki, "Characterizing and modeling mechanical properties and onset of short circuit for three types of lithium-ion pouch cells." *J. Power Sources*, **247**, 503 (2014).
51. LS-DYNA Consistent units, "LS-DYNA support." (Accessed January 2017) (2017) (http://www.dynasupport.com/howtos/general/consistent-units).
52. S. P. V. Nadimpalli, V. A. Sethuraman, D. P. Abraham, A. F. Bower, and P. R. Guduru, "Stress evolution in lithium-ion composite electrodes during electrochemical cycling and resulting internal pressures on the cell casing." *J. Electrochem. Soc.*, **162**, A2656 (2015).
53. B. Croop and H. Lobo, "Selecting material models for the simulation of foams in LS-DYNA." *7th European LS-DYNA Conference, 2009. DYNAmore GmbH* (2009).